Self-Assembly of Amido-Ended Hyperbranched Polyester Films with a Highly Ordered Dendritic Structure

Daohong Zhang,*[,†] Zhicai Xu,[†] Junna Li,[†] Sufang Chen,[‡] Juan Cheng,[†] Aiqing Zhang,[†] Shenghui Chen,[†] and Menghe Miao*[,§]

[†]Key Laboratory of Catalysis and Materials Science of the State Ethnic Affairs Commission & Ministry of Education, South-central University for Nationalities, Wuhan, Hubei 430074, China

[‡]Key Laboratory for Green Chemical Process of Ministry of Education, Wuhan Institute of Technology, Wuhan, Hubei 430073, China

[§]CSIRO Materials Science and Engineering, Belmont, Victoria 3216, Australia

Ⓢ Supporting Information

ABSTRACT: Self-assemblies fabricated from dendrimers and amphiphilic polymers have demonstrated remarkable performances and a wide range of applications. Direct self-assembly of hyperbranched polymers into highly ordered macrostructures with heat-resistance remains a big challenge due to the weak amphiphilicity of the polymers. Here, we report the self-assembly of amphiphilic amido-ended hyperbranched polyester (HTDA-2) into milli-meter-size dendritic films using combined hydrogen bond interaction and solvent induction. The self-assembly process and mechanism have been studied. Hydrogen bond interaction between amido-ended groups assists the aggregation of inner and outer chains of the HTDA-2, resulting in phase separation and micelle formation. Some micelles attach to and grow on the glass substrate like seedlings. Other micelles move to the seedlings and connect with their branches via solvent induction and hydrogen bond interaction, leading to the fabrication of highly ordered crystalline dendritic films that show high heat-resistance. HTDA-2 can further self-assemble into sheet crystals on the dendritic films.
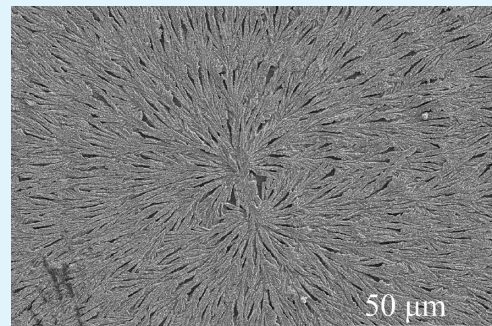
KEYWORDS: hyperbranched polymers, self-assembly, dendritic films, hydrogen bond

1. INTRODUCTION

Molecular self-assembly[1,2] is ubiquitous in nature. It has attracted a great deal of interest in recent years not only because of its fundamental importance in understanding cellular evolution but also for its applications in mimicking biological functions and constructing smart nanomaterials. When compared with small-molecular aggregates obtained in bulk and in aqueous solutions,[3] such as spherical micelles, lamellae, and vesicles, polymer aggregates exhibit high stability and durability because of their mechanical and physical properties. Therefore, polymer self-assembly has been an area of intense research, not only out of academic interest but also because of their potential applications[4−7] in biomedicine, biomaterials, microelectronics, photoelectric materials, catalysts, etc. Hyper-branched polymers (HBPs) as the fourth-generation polymers after linear, branched, and cross-linking polymers have demonstrated superior properties (non/low-entanglement, low solution/melted viscosity, good solubility, compact structure, and possessing a large number of terminal functional groups) and can be fabricated by simple one-pot reaction synthesis processes.[8,9] In comparison to traditional self-assembly of linear block copolymers, HBPs have shown some unique behaviors, including structural diversities, self-assem-bling, unique mechanical properties, excellent template ability, facile functionalization, and smart responses.[10,11]

Like block polymers, the amphiphilic property of HBPs is a crucial factor for achieving stable self-assemblies. Amphiphilic HBPs have been the dominant candidate for HBP self-assembly. There are two types of amphiphilic HBPs, one consisting of hydrophilic linear arms and hydrophobic hyperbranched cores, and the other possessing just the reverse structure. The amphiphilic HBPs reported so far[6,12,13] are only a minority of the HBPs that can be self-assembled into micelles, fibers, tubes, vesicles, films and large compound vesicles (LCVs) using interfacial/surface or selective solvent induc-tion[7,13] within a narrow band of hydrophilic/hydrophobic segment ratios. Considerable efforts have been devoted to the self-assembly of amphiphilic HBPs and their applica-tions[6,7,14−16] such as biomaterials, drug delivery and reaction vessels for charge storage.[6] However, the tedious synthetic processes of these amphiphilic HBPs, such as grafting modification and copolymerization by reversible addition-

Scheme 1. Scheme of HTDA-2 Synthesis
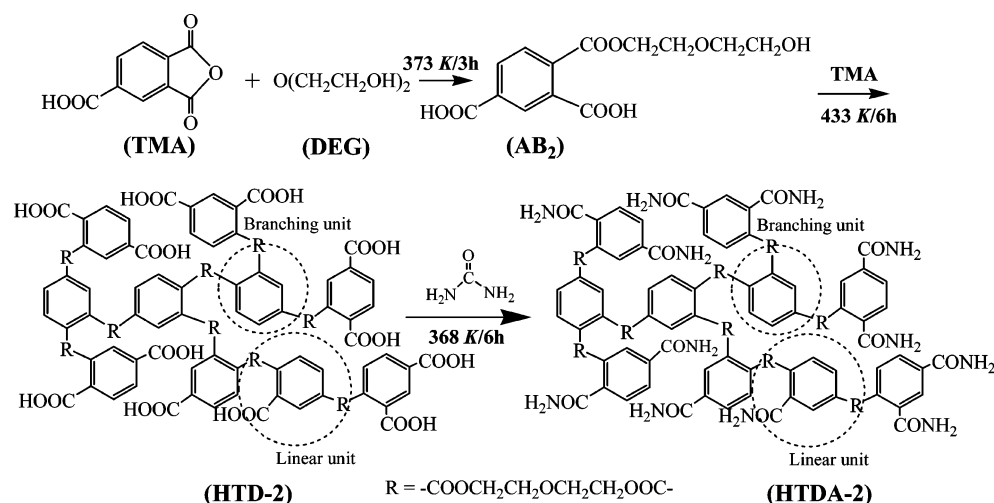
tragmentation chain transfer polymerization (RAFT) process,[6,7] have hampered their adoption. It remains a challenge to assemble nonamphiphilic HBPs (which include the majority of HBPs) directly into ordered supramolecular structures. The self-assembly of nonamphiphilic HBPs,[17,18] including HBPs with carboxyl, hydroxyl, vinyl, and amino-ended groups, is receiving increasingly great attention because of their much easier synthesis processes based on one-pot or pseudo-one-step methods[9] and their greater potential for applications. The functional terminal groups of nonamphiphilic HBPs provide unique properties for encapsulating small molecules or inorganic nanoparticles to form self-assembled structures.[9,10]

The self-assembly mechanism of honeycomb morphology[19,20] and mesoscopic patterns[21] through surface/interfacial self-assembly of amphiphilic hyperbranched polymers or star-polymers has been studied. Solvent evaporation changes the characteristics of the solvent dramatically and induces phase inversion and aggregation of the hydrophobic shell of the core–shell amphiphilic unimolecular micelles.[20] However, nonamphiphilic HBPs are very difficult to self-assemble directly into ordered supramolecular structures on surface and in solution. A couple of years ago, we reported that platinum[17] and copper[18] ions could induce carboxyl-ended HBP self-assembly to form ordered microrods and treelike aggregates on the surface of glass substrates. Platinum ion could also induce carboxyl-ended HBP in a mixed solvent of chloroform and ethanol to self-assemble and form micrometer-sized lamellar films with crystalline and amorphous domains.[22] The self-assemblies containing platinum ion showed much higher catalytic activity for hydrosilylation than traditional homogeneous platinum catalyst.[17,22] In addition, modified HBPs[23] have been used as macromolecular ligands for the anticancer drug cisplatin (cis-diamminedichloroplatinum). Fabricating regular supramolecular structures by direct self-assembly of non-amphiphilic HBPs remains to be a major challenge because of their weak amphiphilicity. A great deal of pioneering work[17,18,22,24,25] has been conducted to increase the amphiphilicity of HBPs, such as metal ion induction method[17,18] and functionalization of nonamphiphilic carboxyl-ended HBPs by amido-ended groups to increase the hydrogen bond interaction between the ended groups and their amphiphilicity.[24,25] Compared with self-assembled carboxyl-ended HBPs produced by metal ion induction, self-assembled amido-ended HBPs

show higher fractal dimension, higher crystallization, and much more compact particle aggregates, indicating improved overall performance. However, both carboxyl-ended and amido-ended HBPs have not been self-assembled into highly ordered porous films. It also remains a major challenge to develop well-controlled shape by direct self-assembly of HBPs. Here for the first time, we report that highly regular dendritic films can be fabricated by direct self-assembly of an amido-ended HBP via solvent induction and hydrogen bond interaction on a glass substrate. A large quantity of sheet crystals has been fabricated by continuous self-assembly of amido-ended HBP on the dendritic films. Characterization shows that the self-assembled dendritic-structure films contain crystal domains and are heat-resistant.

2. EXPERIMENTAL SECTION

2.1. Materials. Trimellitic anhydride (TMA), xylene, diethylene glycol (DEG), tetrabutyl titanate (TBT), urea, triethylamine, isopropanol, chloroform, tetrahydrofuran (THF), and dimethylformamide (DMF) were all of analytical grade and sourced from Shanghai Chemical Reagent Co., Ltd. These chemicals were used in this study without further purification unless noted.

2.2. Preparation of HTDA-2. The synthesis of amido-ended hyperbranched polyester (HTDA-2) is shown in Scheme 1. Carboxyl-ended hyperbranched polyester (HTD-2) containing 12 molar carboxyl groups with number-average molecular weight ($\bar{M}_n$) of about 4260 g/mol and polymerization distribution index (PDI) of about 2.23 from Gel Permeation Chromatography (GPC) was prepared using a previously reported process.[26,27] Characteristic bands of HTD-2 in FT-IR (KCl, cm^{-1}) are 3300–3500 (s, −OH), 1730 (s, −COO−), 1660 (s, −COOH). ^{1}H NMR of HTD-2 (DMSO-d6, ppm) are δ 4.36−4.38 (−COOCH$_2$−), 3.67−3.74 (−CH$_2$OCH$_2$−), 7.75−8.22 (−C$_6$H$_3$).

HTD-2 (3.5 g), urea (2.4 g), triethylamine (20 g) and deionized water (20 mL) were added to a flask to react for about 6 h at 368 K under mechanical stirring. The resulting solution was put in a separation funnel for lamination. The solvent in the up-layer of yellow solution was removed under a pressure of 3−5 mmHg at 363 K for 30 min. This gave a powder solid, which proved to be amido-ended hyperbranched polyester (HTDA-2). Characteristic bands of HTDA-2 in FT-IR (KCl, cm^{-1}) are 3460 and 3260 (s, -NH$_2$), 1730 (s, −COO−), 1622 (s, −CONH$_2$), 1370 (s, −C−N−). ^{1}H NMR of HTDA-2 (DMSO-d6, ppm) are 3.31−4.18 (−COOCH$_2$CH$_2$O−), δ 6.44−6.70 (−CONH$_2$), 7.74−8.27 (−C$_6$H$_3$). HTDA-2 was synthesized using a reaction between excess urea and HTD-2 for complete conversion of HTD-2. Therefore, the degree of branching of HTDA-2

is similar to that of HTD-2. $\bar{M}_n$ of HTDA-2 is about 4250 g/mol according to its chemical structure difference from HTD-2. The disappearance of the characteristic peak at ~12 ppm in ^{1}H NMR demonstrates its free of residual carboxyl groups.

2.3. Self-Assembly of HTDA-2. In a typical experiment, HTDA-2 (0.1 g) was dispersed in solvent (9.9 g) and followed by ultrasonication for 20 min. The solution was dropped on a clean surface of glass substrate to allow for self-assembly under controlled temperature and relative humidity. The morphology of the self-assemblies was measured in real time using optical microscopy (OM) under controlled temperature and relative humidity.

2.4. Characterization. FT-IR measurements were performed on a Bruker Vector 33 spectrometer using sealed cell (KBr 0.5 mm). ^{1}H NMR measurements was conducted on an AVANCE III-400 (Bruker) nuclear magnetic resonance spectrometer using DMSO-d6 as solvent. A low-voltage scanning electron microscope (SEM, XL-30FEG, Philip) and a transmission/reflection polarizing optical microscope (TRPOM, XPV-203E, Shanghai Changfang Optical Instrument Co. Ltd., China) equipped with a thermal platform were used to examine the morphology of the resulting self-assemblies. X-ray diffraction (XRD) patterns were obtained using a Bruker-D8 diffractometer with monochromatized Cu Kα radiation (λ = 1.54 Å) at 40 kV and 40 mA. The surface compositions of the samples were determined using a Vacuum Generator Mutilab 2000 X-ray photoelectron spectrometer (XPS). The C 1s peak of the contamination carbon (284.6 eV) was used as internal standard. Differential scanning calorimetry (DSC) was performed at a heating rate of 5 K/min on a NETZSCH DSC204 F1 differential scanning calorimeter using 1.8−3.0 mg samples placed in standard aluminum pans. Dynamic light scattering (DLS) measurements of samples with a concentration of 1.0 mg/mL were performed on a ZetaSizer Nano ZS90 (Malvern Instrument, Worcs, UK) equipped with 4 mW He−Ne Laser at ~25.0 °C and a scattering angle of 90°. The apparent z-average hydrodynamic diameter (D_h) and polydispersity index (PDI) were calculated using dispersion technology software supplied by Malvern.

3. RESULTS AND DISCUSSION

3.1. Fabrication of Dendritic Films. The morphology of thermodynamically stable supramolecular structures is tuned by the free energy of the system from three contributions, including the stretching of the core-forming blocks, the interfacial tension between the micelle core and the solvent outside the core, and the repulsive interactions among micelles.[28,29] Other crucial factors that influence the self-assembly morphology, including end-group composition, types of solvent, temperature and relative humidity, are discussed in the Supporting Information. HTDA-2 solution can be self-assembled into regular dendritic structures (see Figure S1b in the Supporting Information) because of its stronger hydrogen bond interaction of the amido groups than carboxyl groups of HTD-2, compared with a flat film (see Figure S1a in the Supporting Information) by self-assembled HTD-2. DMF or DMAc can dissolve the peripheral segments of amido-ended groups rather than the core segments because of similar solubility property (see Figure S2 in the Supporting Information), resulting in phase-separation between the core and the peripheral segments and the formation of micelles. Low relative humidity and low temperature are necessary condition for the fabrication of treelike self-assemblies, affecting the movement of micelles and the vaporization of DMF in Figures S3 and S4 in the Supporting Information.

On the basis of these detailed investigation, the optimum conditions for fabricating self-assembled dendritic films were derived. At the self-assembling conditions of 298 K and 20% relative humidity (RH), HTDA-2/DMF solutions at different

concentrations were added to different glass substrates for self-assembly. The resulting morphologies are shown in Figure 1.
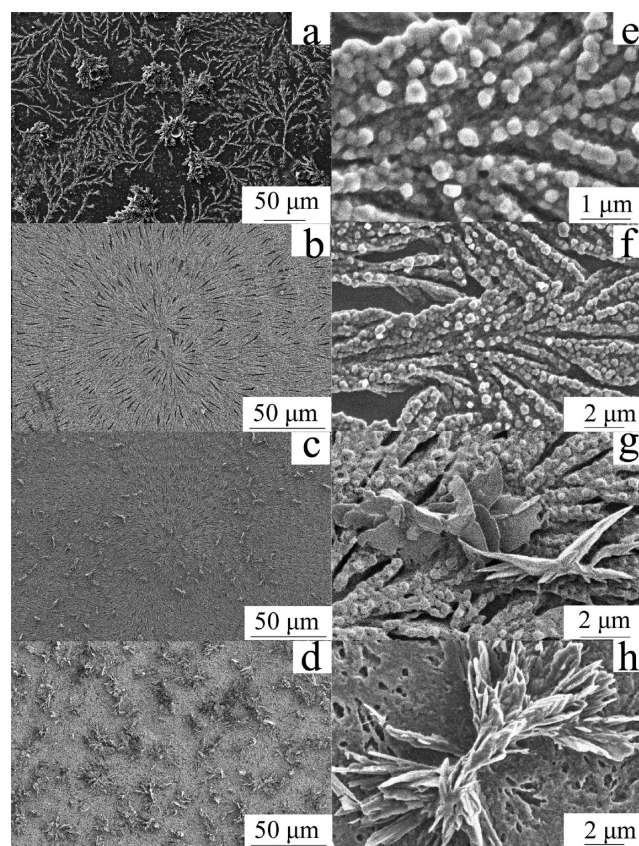

Figure 1. SEM micrographs of self-assembled HTDA-2 at different concentrations: (a) 0.5, (b, e, f) 1, (c, g) 3, and (d, h) 5 wt %.

When HTDA-2 concentration was increased from 0.50 to 5.00 wt % (including intermediate concentrations at 1 and 3 wt %), the morphology of the resulting self-assemblies changed from ordered aggregates of individual tree-like structures (Figure 1a) to a single dendritic film (Figure 1b), and finally to a microporous film with flowerlike crystals (Figure 1c, d). All these self-assemblies were composed of aggregates of micelle particles (Figure 1) with diameters from about 200 to 500 nm. Sphere-like particles appeared clearly on the surface of glass substrates at higher magnifications in Figure 1e−g. Isolated but ordered treelike structures (Figure 1a) were observed in the self-assembly 0.50 wt % HTDA-2 solution because there was insufficient time for the micelle particles to aggregate. At higher HTDA-2 concentration, the treelike structures were self-assembled into an interconnected dendritic film (Figure 1b−d) with some micelle particles being squeezed out from the dendritic film, and consequently the micelle particles self-assembled into sheet crystals on the film (Figure 1g, h). Figure 2a is a local magnification of Figure 1h. Images b and c in Figure 2 shows self-assembled morphologies achieved from three cycles of self-assembling of 1 wt % HTDA-2 with an interval of 24 h between cycles. The microstructures of the sheet crystals (Figure 2) were distinctly different from the self-assembled films (Figure 1b) because they followed different self-assembling or aggregating mechanisms. The self-assembly and crystallization of the HTDA-2 on glass substrate and the self-assembly of the films may be considered to be

16377

dx.doi.org/10.1021/am504705c | *ACS Appl. Mater. Interfaces* 2014, 6, 16375−16383

Figure 2. SEM micrographs of self-assembled HTDA-2/DMF at different concentrations and cycles of treatments: (a) 5 wt %, (b, c) 1 wt %/3 cycles.

heterogeneous and homogeneous nucleation processes,[30] respectively. Heterogeneous nucleation involves the formation of small crystalline regions on or near a surface initiated at defects or impurities extrinsic to the pure material[31,32] in Figure 1b. On the other hand, homogeneous nucleation involves the creation of small regions of crystalline phase as the root for sheet crystal growth, as in Figure 1h and Figure 2b, c, which is less common but intrinsic to the polymer.

3.2. Properties of Dendritic Films.
Self-assemblies obtained previously by self-assembling amphiphilic HBPs were amorphous[6,10,33,34] without incorporating crystalline polyethylene glycol (PEG)[2] and polyhedral oligomeric silsesquioxane (POSS)[35] segments, resulting in poor heat-resistance. The self-assembled materials recently fabricated in our lab by platinum[17] and copper[18] ion-induced self-assembly of carboxyl-ended hyperbranched polyester also contain crystal structures. The XRD spectrum of the amorphous HTD-2 has a broad peak (2θ) between 18 and 30° and a strong Bragg reflection peak at 20° corresponding to urea crystals, while the XRD spectrum of crystal HTDA-2 contains typical reflection peaks marked with rectangular signals appear at 2θ ranges 9–10, 12–13, 19–21, 23–24, and 27–28°, as shown in Figure 3.
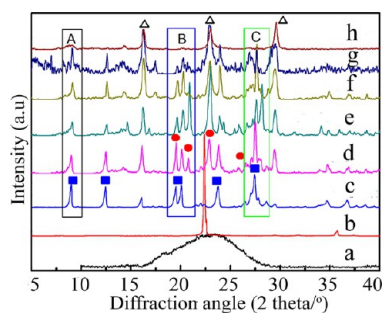

Figure 3. XRD spectra of (a) HTD-2, (b) urea, (c) HTDA-2, (d) self-assembled HTDA-2/298 K, (e) self-assembled HTDA-2/298 K/3 cycles, (f) self-assembled HTDA-2 treated at 373 K, (g) self-assembled HTDA-2 treated at 393 K, and (h) self-assembled HTDA-2 treated at 423 K. A region (7–9°), B region (18–22°), and C region (26–29°).

These typical crystal peaks are assigned to the crystal structures of the amido-ended group fragments.[36] The results suggest that the HTDA-2 might have crystallized into a close-to-hexagon packing of polymer chains and that the HTDA-2 consists of stacked hydrogen-bonded sheets, in which the polymer chains are arranged side-by-side.[37] Crystallization of the amido-ended groups in the HTDA-2 may be induced by solvent triethyl-amine because the latter has similar polarity as the amido-ended groups. The solvent-induced crystallization is associated with the selective interaction of solvent with the amido (−CONH₂)

part of the HTDA-2 molecule. This demonstrates that the interaction is directly responsible for the increased crystallization.[38] The XRD spectra of the self-assembled HTDA-2 in Figure 3d-h show that some new refraction peaks have appeared at $2\theta \approx$ 20.8, 22.9, and 29.5°, indicating new crystal structures. The appearance of melting peaks during heating and the absence of crystal peaks during cooling in Figure 4 suggest
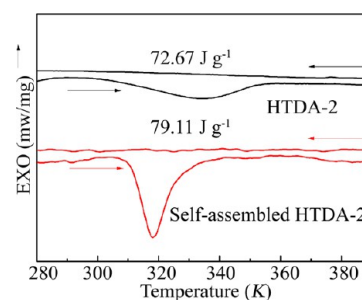

Figure 4. DSC thermograms of amorphous HTDA-2 and self-assembled HTDA-2.

that the crystal structure were formed during self-assembly. The increase in melting heat of the self-assembled HTDA-2 (79.11 J g^{-1}) over the HTDA-2 (72.69 J g^{-1}) indicates that the surface self-assembly favors crystallization of HTDA-2. The three distinct diffraction peaks marked with triangles at 19.3, 22.9, and 29.6° in Figure 3h are similar to those of poly(aryl ketone)[39,40] at 19.2–19.4, 22.8–23.0, and 29.4–29.8°, respectively. These peaks may, therefore, be attributed to the crystal structure of poly(phenyl ester) based TMA in the HTDA-2. The four diffraction peaks marked with circles in Figure 3d can be attributed to the crystal structure of ethylene oxide chains.[30] All three diffraction peaks at ~20.9, 23.0, and 28.2° in Figure 3e are higher than the corresponding peaks in Figure 3d, suggesting an increase in crystallization degree as a result of the continuation of self-assembling HTDA-2 on the self-assembled dendritic film. Besides their different nucleation crystallization processes, the hard segments formed by hydrogen bond interaction between amide chains promote crystallization of the self-assembled HTDA-2,[41] resulting in changes in the corresponding crystal peak area at the 2θ ranges of 18–22 and 26–29°. Increasing the treatment temperature applied to the self-assembled HTDA-2 dendritic films caused hydrogen bonds to break off and the corresponding crystals to melt gradually. This weakens the relationship between the crystal peaks and the hydrogen bonds. Table 1 shows the crystal peak to area ratio (B_{ar}) between B region (18–22°) and A region (the unchanged basic peak in Figure 3) and the ratio (C_{ar}) between C region (26–29°) and A region. These area

Table 1. Relationship between Crystal Peak Area Ratio and Hydrogen Bond Interaction

samples	B_{ar} (area ratio between B region and A region)	C_{ar} (area ratio between C region and A region)
HTDA-2	0.92	1.42
self-assembled HTDA-2/298K	2.74	6.48
self-assembled HTDA-2/298K/ 3cycles	3.85	7.20
self-assembled HTDA-2/373K	1.38	5.90
self-assembled HTDA-2/393K	0.66	2.76
self-assembled HTDA-2/423K	0.22	1.58

ratios point to a trend of steady decrease in crystallization degree as the treatment temperature increases. Both B_{ar} and C_{ar} for self-assembled HTDA-2 at 298 K are greater than their respective ratios for HTDA-2, respectively, indicating an increase in crystallization induced hydrogen bond interaction due to surface self-assembly. The dendritic films fabricated by multicycle self-assembly also possess much higher B_{ar} and C_{ar} values (higher crystallization degree) than that of the HTDA-2 films fabricated by one-cycle self-assembly as shown in Table 1. This is in agreement with the morphology shown in the SEM images. Figure 2b shows much more sheet crystals than Figure 1b.

Many self-assembled structures are soft amorphous materials with low glass transition temperature.[42] As a result, the morphology of these self-assemblies would distort once the ambient temperature increases. Fabrication of self-assemblies with high temperature stability is a challenge. The dendritic films fabricated by self-assembling 1 wt % HTDA-2/DMF solution at 298 K and 20% RH was directly placed on a heating stage in an optical microscope for in situ observation. The stage was heated at a rate of 2 K/min from 298 to 433 K. The morphologies taken at 10 min intervals (corresponding to 20 K temperature steps) are shown in Figure 5.

The morphologies of the self-assemblies show little change as the treatment temperature increased from 298 to 373 K. Then the morphological patterns became unclear and the formed dendrites started to break up gradually as the temperature was raised from 393 to 433 K. This is because the hydrogen bonds start to break up and the crystal structure starts to melt. This change of crystal structure with treatment temperature is also consistent with that discussed earlier in relation to Figure 3 and Table 1.

3.3. Self-Assembly Mechanism of Dendritic Films. It is well-recognized that the band envelope encompassing the N−H stretching mode is composed of two main contributions, i.e., "free" (non-hydrogen bonded) and hydrogen-bonded N−H groups.[43] The infrared bands at 3460 and 3327 cm^{-1} in Figure 6 can be assigned to the N−H stretching modes of the "free" and hydrogen bonded N−H groups of the self-assemblies, respectively.[41] The mean strength of the hydrogen bonds diminishes gradually with increasing temperature from 298 K to 353 K, indicating that the absorption peak of hydrogen bonded N−H groups shifted from 3327 to 3336 cm^{-1} and finally disappeared.
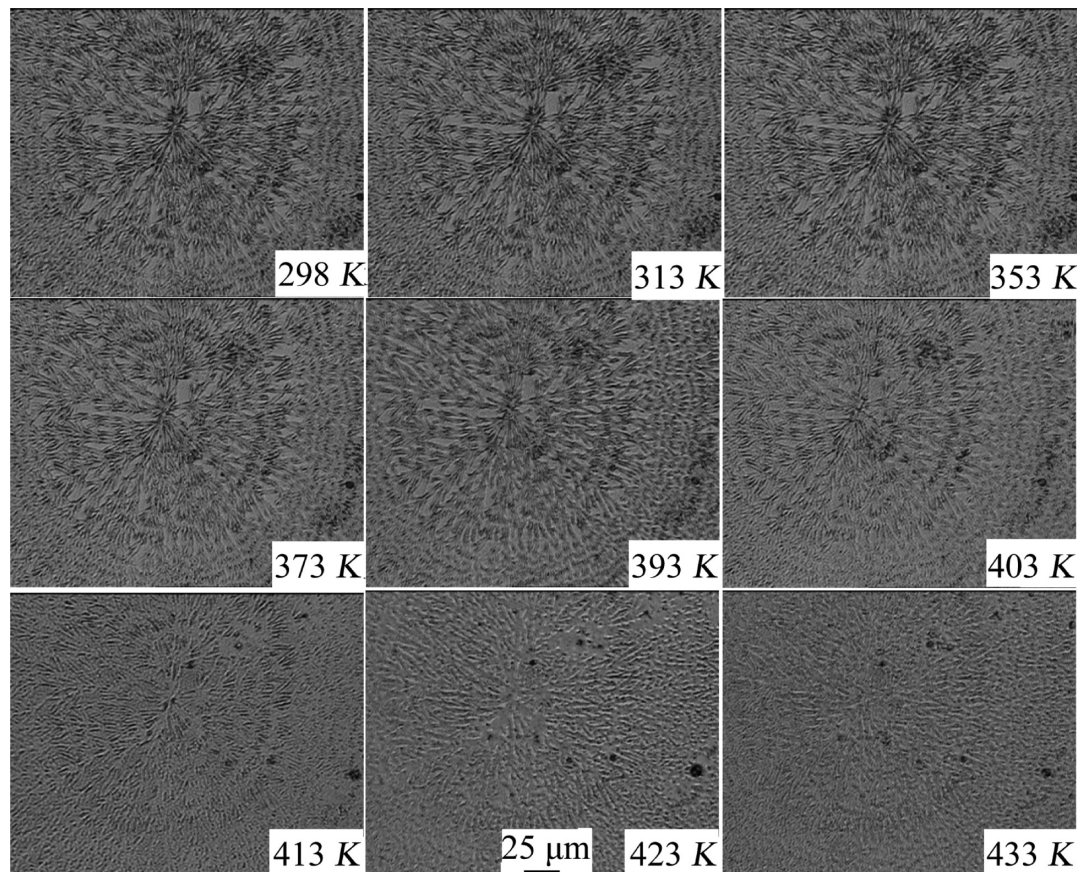

Figure 5. Effect of increasing temperature on morphology of self-assembled HTDA-2. All images share the same scale bar shown in the bottom row.
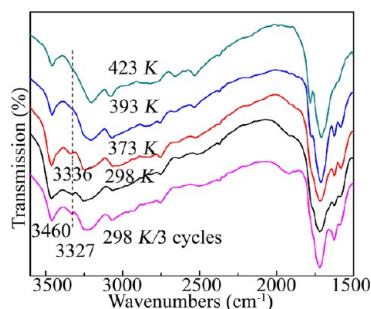
Figure 6. FT-IR spectra of self-assembled HTDA-2 treated at different temperatures and numbers of treatment cycles.

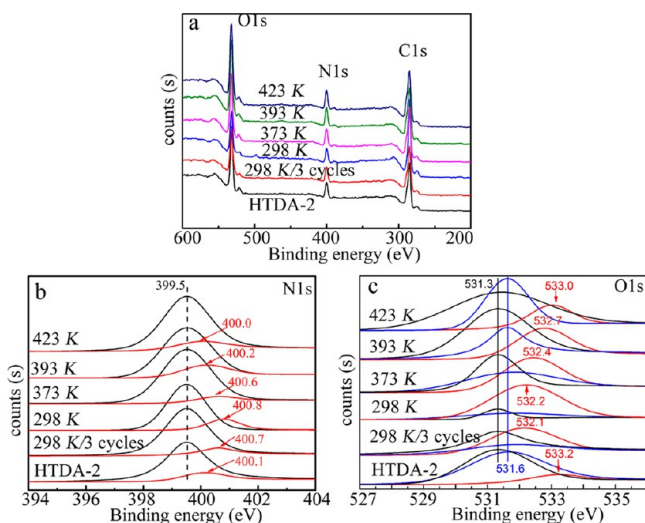The XPS spectra of HTDA-2 and self-assembled HTDA-2 are shown in Figure 7. Peaks of binding energy at ~285, 399,

Figure 7. (a) C 1s, (b) N 1s, and (c) O 1s XPS spectra of self-assembled HTDA-2 at different treatment temperatures.

and 532 eV in Figure 7a are attributed to C 1s, N 1s and O 1s electrons, respectively. Each of the N 1s peaks can be deconvoluted into two peaks, attributed to "free" (non-hydrogen-bonded) and hydrogen-bonded amido groups (−CON−). The binding energies of N 1s electron at 399.5 eV and in the range 400.1− 400.8 eV in Figure 7b are assigned to the "free" and hydrogen bonded amido groups of the self-assemblies, respectively. The N1s peaks of the hydrogen bonded amido groups shifted gradually from 400.7−400.8 to 400 eV in Figure 7b as the treatment temperature increased, indicating that nitrogen in the self-assemblies became slightly less electropositive as the hydrogen bond interaction weakened.[44]

Peaks of binding energy at ~531.3 and 531.6 eV in Figure 7c are attributed to O 1s electrons in ether (−C−O−C−) and ester (−COOC−) groups, respectively, and the peaks of binding energy at ~532−533 eV could be assigned to O 1s electrons in the amido groups (−CON−). When the treatment temperature on the self-assembled HTDA-2 was increased, both binding energies at 531.3 and 531.6 eV remained unchanged, but the binding energy of O 1s electrons in amido groups increased from 532.2 to 533.0 eV, suggesting that hydrogen-bond interaction had weakened.[45]

The solvent-induced surface self-assembly of HBPs or star polymers without metal ions is usually considered to be a combined honeycomb film fabrication process that includes

solvent evaporation, water condensation, and core−shell micelle aggregation.[19−21,46] The mechanism for metal-ion-induced surface self-assembly of HBPs is considered to include the following processes: metal-ion coordination, micelle formation, solvent evaporation, diffusion-limited aggregation of particles, and finally formation of a self-assembly of certain morphology, for example, 1D microrodlike[17] or 2D tree-like.[24,25] To explain the self-assembly mechanism of the new dendritic films, we examined, using in situ transmission/reflection polarizing optical microscope (TRPOM), the growth process of self-assembling HTDA-2/DMF solution with 1 wt % concentration on the surface of glass substrates at 298 K and 20% RH. The morphologies of the self-assemblies in time sequence are shown in Figure 8. The morphology study shows clearly that the highly ordered dendritic films are formed by assembling many treelike branches side-by-side, very similar to the fabrication of self-assembled conjugated polymers[47] and dendrimers.[48] It is therefore conclude that the self-assembly process of the highly ordered dendritic films can be explained by the particle diffusion-limited aggregation (DLA) theory.[49]

On the basis of the above results and analyses, a mechanism for the growth and self-assembly of the dendritic films is proposed as follows:

(1) Because the solubility parameter of DMF (24.80 $(J/cm^3)^{0.5}$) is much closer to that of the peripheral amido-ended groups of HTDA-2 (25.24 $(J/cm^3)^{0.5}$) than to that of the core chains of HTDA-2 (19.42 $(J/cm^3)^{0.5}$), the condition favors phase-separation between the peripheral amido-ended groups and the core chains, and the aggregation and final formation of micelles, as discussed in detail in the Supporting Information and substantiated by the apparent z-average hydrodynamic diameter of HTDA-2 (about 839.1 nm) in Figure S5 in the Supporting Information.

(2) After the HTDA-2 solution consisting of micelles spreads homogeneously on the substrate, the micelles start to form aggregates at different locations. As the solvent evaporates and the temperature of the aggregates decreases, water droplets are formed on the surface of the aggregates,[46] which causes the aggregates to shrink. The evaporation of DMF drives the aggregates to move together and rearrange through hydrogen bond inter-action, resulting in root formation at the self-assembly time of ~83 min, as shown in Figure 8. With further evaporation of the DMF, some aggregates in the nearby region move and attach to the root. This results in the formation of a "sapling", which grows over time and finally becomes a mature tree.

(3) Alternatively, the aggregates may be regarded as particles in the diffusion-limited aggregation (DLA) model,[49] in which the root forms the core of the self-assembly system. The root situates at the origin of a region and the individual particles (or aggregate) are scattered over the region. The particles move randomly as DMF evaporates until they reach a site adjacent to the root. One moving particle touches and attaches to the root to become a sapling. In the next moment, another randomly moving particle comes over and attaches to the sapling. In this way, a treelike structure is gradually formed. This process is evidenced by the appearance of aggregates (that are about 300−500 nm in diameter, as shown in Figure 1e). The exposed ends of the tree-like structure tend to grow
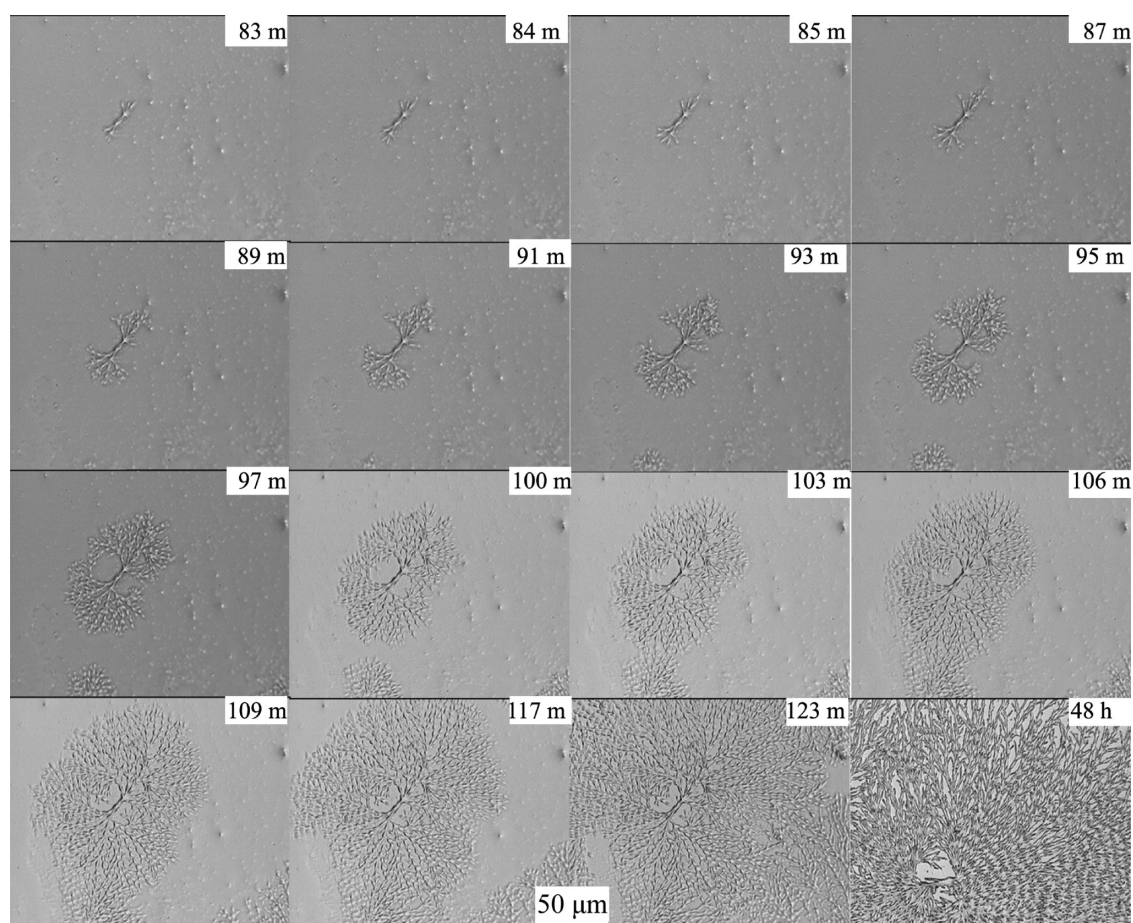
Figure 8. Optical micrographs of self-assembled HTDA-2 in time sequence. All images share the same scale bar.

more rapidly than sites near the center because the central sites situate in the "shadow". The branches grow and flourish as they connect with neighboring particles. Finally, all the particles in the region are attached to the treelike structure and a dendritic film is produced.

4. CONCLUSIONS

We have reported a novel method of self-assembling highly ordered dendritic films from amphiphilic amido-ended hyper-branched polyester based on solvent induction and hydrogen bond interaction. A large quantity of sheet crystals has been fabricated by continuous self-assembly of amido-ended HBP on the dendritic films. Factors influencing the morphology of the self-assembled highly ordered dendritic film, including solvent type and concentration, temperature and relative humidity, and treatment time, were investigated using OM and SEM techniques. A self-assembly mechanism has been proposed based on the DLA theory and evidence from FT-IR, XPS, and DLS experiments. The resultant highly ordered crystalline dendritic films have excellent heat-resistance.

■ ASSOCIATED CONTENT

Ⓢ Supporting Information

Factors influencing self-assembled morphology. This material is available free of charge via the Internet at http://pubs.acs.org.

■ AUTHOR INFORMATION

Corresponding Authors
*E-mail: zhangdh27@163.com.
*E-mail: Menghe.Miao@csiro.au.

Notes
The authors declare no competing financial interest.

■ ACKNOWLEDGMENTS

■ REFERENCES

(1) Mai, Y.; Eisenberg, A. Self-Assembly of Block Copolymers. *Chem. Soc. Rev.* **2012**, *41*, 5969−5985.
(2) Samuel, A. Z.; Ramakrishnan, S. Janus Hybramers: Self-Adapting Amphiphilic Hyperbranched Polymers. *Macromolecules* **2012**, *45*, 2348−2358.
(3) Fong, C.; Le, T.; Drummond, C. J. Lyotropic Liquid Crystal Engineering−Ordered Nanostructured Small Molecule Amphiphile Self-Assembly Materials by Design. *Chem. Soc. Rev.* **2012**, *41*, 1297−1322.
(4) Mann, S. Self-Assembly and Transformation of Hybrid Nano-Objects and Nanostructures Under Equilibrium and Non-Equilibrium Conditions. *Nat. Mater.* **2009**, *8*, 781−792.

(5) Dhar, J.; Patil, S. Self-Assembly and Catalytic Activity of Metal Nanoparticles Immobilized in Polymer Membrane Prepared via Layer-by-Layer Approach. *ACS Appl. Mater. Interfaces* **2012**, *4*, 1803−1812.

(6) Peleshanko, S.; Tsukruk, V. V. Assembling Hyperbranched Polymerics. *J. Polym. Sci., Part B: Polym. Phys.* **2012**, *50*, 83−100.

(7) Chen, S.; Cheng, S. X.; Zhuo, R. X. Self-Assembly Strategy for the Preparation of Polymer-Based Nanoparticles for Drug and Gene Delivery. *Macromol. Biosci.* **2011**, *11*, 576−589.

(8) Konkolewicz, D.; Monteiro, M. J.; Perrier, S. B. Dendritic and Hyperbranched Polymers from Macromolecular Units: Elegant Approaches to the Synthesis of Functional Polymers. *Macromolecules* **2011**, *44*, 7067−7087.

(9) Voit, B. I.; Lederer, A. Hyperbranched and Highly Branched Polymer Architectures—Synthetic Strategies and Major Characterization Aspects. *Chem. Rev.* **2009**, *109*, 5924−5973.

(10) Zhou, Y.; Yan, D. Supramolecular Self-Assembly of Amphiphilic Hyperbranched Polymers at All Scales and Dimensions: Progress, Characteristics and Perspectives. *Chem. Commun.* **2009**, *10*, 1172−1188.

(11) Jin, H.; Huang, W.; Zhu, X.; Zhou, Y.; Yan, D. Biocompatible or Biodegradable Hyperbranched Polymers: from Self-Assembly to Cytomimetic Applications. *Chem. Soc. Rev.* **2012**, *41*, 5986−5997.

(12) Percec, V.; Wilson, D. A.; Leowanawat, P.; Wilson, C. J.; Hughes, A. D.; Kaucher, M. S.; Hammer, D. A.; Levine, D. H.; Kim, A. J.; Bates, F. S. Self-Assembly of Janus Dendrimers into Uniform Dendrimersomes and Other Complex Architectures. *Science* **2010**, *328*, 1009−1014.

(13) Zhou, Y.; Huang, W.; Liu, J.; Zhu, X.; Yan, D. Self-Assembly of Hyperbranched Polymers and Its Biomedical Applications. *Adv. Mater.* **2010**, *22*, 4567−4590.

(14) Chen, C.; Liu, G.; Liu, X.; Pang, S.; Zhu, C.; Lv, L.; Ji, J. Photo-Responsive, Biocompatible Polymeric Micelles Self-Assembled from Hyperbranched Polyphosphate-Based Polymers. *Polym. Chem.* **2011**, *2*, 1389−1397.

(15) Wang, R.; Jiang, X.; Yu, B.; Yin, J. Stimuli-Responsive Microgels Formed by Hyperbranched Poly(Ether Amine) Decorated with Platinum Nanoparticles. *Soft Matter* **2011**, *7*, 8619−8627.

(16) Tao, W.; Liu, Y.; Jiang, B.; Yu, S.; Huang, W.; Zhou, Y.; Yan, D. A Linear-Hyperbranched Supramolecular Amphiphile and Its Self-Assembly into Vesicles with Great Ductility. *J. Am. Chem. Soc.* **2012**, *134*, 762−764.

(17) Zhang, D.; Wang, J.; Chen, S.; Cheng, X.; Li, T.; Zhang, J.; Zhang, A. Surface Hybrid Self-Assembly, Mechanism and Crystalline Behavior of Carboxyl-Ended Hyperbranched Polyester/Platinum Complex. *Langmuir* **2012**, *28*, 16772−16781.

(18) Zhang, D.; Li, J.; Chen, S.; Li, T.; Zhou, J.; Cheng, X.; Zhang, A. Hybrid Self-Assembly, Crystal, and Fractal Behavior of a Carboxy-Ended Hyperbranched Polyester/Copper Complex. *Macromol. Chem. Phys.* **2013**, *214*, 370−377.

(19) Widawski, G.; Rawiso, M.; François, B. Self-Organized Honeycomb Morphology Of Star-Polymer Polystyrene Films. *Nature* **1994**, *369*, 387−389.

(20) Liu, C.; Gao, C.; Yan, D. Honeycomb-Patterned Photoluminescent Films Fabricated by Self-Assembly of Hyperbranched Polymers. *Angew. Chem., Int. Ed.* **2007**, *46*, 4128−4131.

(21) Maruyama, N.; Koito, T.; Nishida, J.; Sawadaishi, T.; Cieren, X.; Ijiro, K.; Karthaus, O.; Shimomura, M. Mesoscopic Patterns of Molecular Aggregates on Solid Substrates. *Thin Solid Films* **1998**, *327*, 854−856.

(22) Zhang, D.; Wang, J.; Chen, S.; Cheng, X.; Li, T.; Zhang, J.; Zhang, A. Hybrid Self-Assembly, Crystal Behavior and Catalytic Activity of Carboxyl-Ended Hyperbranched Polyester /Platinum Complex. *Sci. Adv. Mater.* **2013**, *6*, 16772−16781.

(23) Haxton, K. J.; Burt, H. M. Hyperbranched Polymers for Controlled Release of Cisplatin. *Dalton T.* **2008**, *43*, 5872−5875.

(24) Zhang, D.; Li, J.; Wang, J.; Chen, S.; Zhou, J.; Li, T.; Zhang, J.; Zhang, A.; Liu, C. 2D Self-Assembly of an Amido-Ended Hyperbranched Polyester Induced by Platinum Ion Coordination Effect. *RSC Adv.* **2013**, *3*, 17073−17080.

(25) Li, J.; Zhang, D.; Li, S.; Xu, Z.; Chen, S.; Li, T.; Zhang, J.; Chen, S.; Zhang, A. 2D Self-Assembly of an Amido-Ended Hydrophilic Hyperbranched Polyester by Copper Ion Induction. *Macromol. Chem. Phys.* **2013**, *214* (15), 1724−1733.

(26) Zhang, D.; Jia, D. Synthesis of Novel Low-Viscosity Liquid Epoxidized Aromatic Hyperbranched Polymers *Europ. Polym. J.* **2006**, *42*, 711−714.

(27) Zhang, D.; Jia, D.; Chen, S. Synthesis and Characterization of Low Viscosity Aromatic Hyperbranched Poly (Trimellitic Anhydride Ethylene Glycol) Ester Epoxy Resin. *Macromol. Chem. Phys.* **2009**, *210*, 1159−1166.

(28) Zhang, L.; Eisenberg, A. Multiple Morphologies and Characteristics of "Crew-Cut" Micelle-Like Aggregates of Polystyrene-b-Poly (Acrylic Acid) Diblock Copolymers in Aqueous Solutions. *J. Am. Chem. Soc.* **1996**, *118*, 3168−3181.

(29) Zhang, L.; Eisenberg, A. Formation of Crew-Cut Aggregates of Various Morphologies From Amphiphilic Block Copolymers in Solution. *Polym. Adv. Technol.* **1998**, *9*, 677−699.

(30) Maiz, J.; Martin, J.; Mijangos, C. Confinement Effects on the Crystallization of Poly (ethylene oxide) Nanotubes. *Langmuir* **2012**, *28*, 12296−12303.

(31) Huang, P.; Zhu, L.; Cheng, S. Z.; Ge, Q.; Quirk, R. P.; Thomas, E. L.; Lotz, B.; Hsiao, B. S.; Liu, L.; Yeh, F. Crystal Orientation Changes in Two-Dimensionally Confined Nanocylinders in a Poly (Ethylene Oxide)-b-Polystyrene/Polystyrene Blend. *Macromolecules* **2001**, *34*, 6649−6657.

(32) Pielichowska, K.; Pielichowski, K. Kinetics of Isothermal and Nonisothermal Crystallization of Poly (ethylene oxide)(PEO) in PEO/Fatty Acid Blends. *J. Macromol. Sci., Part B* **2011**, *50*, 1714−1738.

(33) Khanna, K.; Varshney, S.; Kakkar, A. Miktoarm Star Polymers: Advances in Synthesis, Self-Assembly, and Applications. *Polym. Chem.* **2010**, *1*, 1171−1185.

(34) Leung, K. C.F.; Lau, K. N. Self-Assembly and Thermodynamic Synthesis of Rotaxane Dendrimers and Related Structures. *Polym. Chem.* **2010**, *1*, 988−1000.

(35) Jiang, B.; Tao, W.; Lu, X.; Liu, Y.; Jin, H.; Pang, Y.; Sun, X.; Yan, D.; Zhou, Y. A POSS-Based Supramolecular Amphiphile and Its Hierarchical Self-Assembly Behaviors. *Macromol. Rapid Commun.* **2012**, *33*, 767−772.

(36) Jasinska, L.; Villani, M.; Wu, J.; van Es, D.; Klop, E.; Rastogi, S.; Koning, C. E. Novel, Fully Biobased Semicrystalline Polyamides. *Macromolecules* **2011**, *44*, 3458−3466.

(37) Jones, N.; Atkins, E.; Hill, M.; Cooper, S.; Franco, L. Chain-folded lamellar crystals of aliphatic polyamides. Investigation of nylons 4 8, 4 10, 4 12, 6 10, 6 12, 6 18 and 8 12. *Polymer* **1997**, *38*, 2689−2699.

(38) Kulshreshtha, A.; Khan, A.; Madan, G. X-ray Diffraction Study Of Solvent-Induced Crystallization In Polyester Filaments. *Polymer* **1978**, *19*, 819−823.

(39) Ji, X. L.; Zhang, W. J.; Na, H.; Qiu, X. P.; Wang, J. Z.; Wu, Z. W.; Mo, Z. S.; Zhang, H. F. Effect of Differences in the Backbone Chemical Environment of Carbonyl and Ether Groups in Poly (Aryl Ether Ketones) on Crystallographic Parameters. *Macromolecules* **1997**, *30*, 4772−4774.

(40) Colquhoun, H. M.; Aldred, P. L.; Zhu, Z.; Williams, D. J. First Structural Analysis of a Naphthalene-Based Poly(ether ketone): Crystal and Molecular Simulation from X-ray Powder Data and Diffraction Modeling. *Macromolecules* **2003**, *36*, 6416−6421.

(41) Xiu, Y.; Zhang, Z.; Wang, D.; Ying, S.; Li, J. Hydrogen Bonding And Crystallization Behaviour Of Segmented Polyurethaneurea: Effects Of Hard Segment Concentration. *Polymer* **1992**, *33*, 1335−1338.

(42) Walther, A.; Müller, A. H. E. Janus Particles: Synthesis, Self-Assembly, Physical Properties, and Applications. *Chem. Rev.* **2013**, *113*, 5194−5261.

(43) Coleman, M. M.; Lee, K. H.; Skrovanek, D. J.; Painter, P. C. Hydrogen Bonding in Polymers. 4. Infrared Temperature Studies of a Simple Polyurethane. *Macromolecules* **1986**, *19*, 2149−2157.

(44) Zhou, X.; Goh, S.; Lee, S.; Tan, K. X-ray Photoelectron Spectroscopic Studies of Interactions Between Poly(p-Vinylphenol) and Poly(Vinylpyridine)s. *Appl. surface Sci.* **1997**, *119*, 60−66.

(45) Liu, S.; Chan, C. M.; Weng, L. T.; Jiang, M. Surface Segregation in Polymer Blends and Interpolymer Complexes with Increasing Hydrogen Bonding Interactions. *J. Polym. Sci., Part B: Polym. Phys.* **2005**, *43*, 1924−1930.

(46) Srinivasarao, M.; Collings, D.; Philips, A.; Patel, S. Three-Dimensionally Ordered Array of Air Bubbles in A Polymer Film. *Science* **2001**, *292*, 79−83.

(47) Gan, H.; Li, Y.; Liu, H.; Wang, S.; Li, C.; Yuan, M.; Liu, X.; Wang, C.; Jiang, L.; Zhu, D. Self-Assembly of Conjugated Polymers and ds-Oligonucleotides Directed Fractal-like Aggregates. *Biomacro-molecules* **2007**, *8*, 1723−1729.

(48) Das, I.; Goel, N.; Agrawal, N. R.; Gupta, S. K. Growth Patterns of Dendrimers and Electric Potential Oscillations during Electro-polymerization of Pyrrole using Mono- and Mixed Surfactants. *J. Phys. Chem. B* **2010**, *114*, 12888−12896.

(49) Witten, T. A., Jr.; Sander, L. M. Diffusion-Limited Aggregation, a Kinetic Critical Phenomenon. *Phys. Rev. Lett.* **1981**, *47* (19), 1400−1403.